UNIVERSITAT POLITÈCNICA DE VALÈNCIA

Escuela Técnica Superior de Ingeniería del Diseño

UNIVERSITAT POLITÈCNICA DE VALÈNCIA

School of Design Engineering

CFD study of the aerodynamics of the Aérospatiale-BAC Concorde

End of Degree Project

Bachelor's Degree in Aerospace Engineering

AUTHOR: Lamuela Dorado, Óscar

Tutor: Margot, Xandra Marcelle

ACADEMIC YEAR: 2022/2023

UNIVERSITAT POLITÈCNICA DE VALÈNCIA

CFD Study of the Aerodynamics of the Aéroespatiale-BAC Concorde

Aerospace Engineering Degree
11982 - Bachelor's Thesis

Óscar Lamuela Dorado
Tutor: Xandra Marcelle Margot

Universitat Politènica de València - ETSID - Junio 2023

Contents

List of Figures

List of Tables

0 Summary

The presented Bachelor's Thesis consist in performing a CFD study on the aerodynamics of the commercial passenger aircraft Concorde, designed and manufactured by Aéroespatiale and British Aircraft Corporation (BAC). This is done in order to obtain a better understanding of the aerodynamic behaviour of delta-shaped wings and the use of Computational Fluid Dynamics tools such as Star-CCM+, which is the one used for this thesis.

To achieve this, the full-scale geometry of a model of the Concorde is taken and simplified to mesh it in Star-CCM+, making a thorough description of the domain used as a basis for the simulations, the initial mesh considered and the solvers used in all of the studied cases. Having done this, the convergence and mesh independence are studied to be sure that the obtained results will be somewhat accurate, indicating when and where issues occurred and how they were solved. Then, simulations at different angles of attack, and sub and supersonic flight conditions, corresponding with the take-off and cruise flight regimes, are performed. After that, the variation with respect to the angle of attack of the lift, drag and moment coefficients are studied for each of these flight regimes, together with any other data useful to the understanding of the obtained results and their validation, as well as any abnormalities found. The next step taken was the validation of all of the obtained results by contrasting it with the theory regarding delta-shaped wings and bibliographical data of the Concorde's aerodynamic performance.

Last, but not least, a discussion of the budget needed to perform the project and its relation to the UN's Sustainable Development Goals are made, followed by a conclusion to close the document.

0 Resumen

El Trabajo de Fin de Grado (TFG) que se presenta consiste en la realización de un estudio con Mecánica de Fluidos Computacional (CFD en inglés) de la aerodinámica del avión comercial de pasajeros Concorde, diseñado y fabricado por Aérospatiale y British Aircraft Corporation (BAC). El fin de este estudio es comprender mejor la aerodinámica de las alas con forma de delta y del uso de las herramientas de CFD como Star-CCM+, que es el programa específico utilizado para este TFG.

Para ello, se toma y simplifica la geometría de un modelo a escala real del Concorde y se malla en Star-CCM+, haciéndose una descripición en detalle del dominio considerado como base para las simulaciones, la malla empleada inicialmente y los *solvers* usados en cada uno de los casos estudiados. Hecho esto, se estudian la convergencia e independencia de malla para asegurarse de que los resultados obtenidos son mínimamente correctos, indicándose dónde y cuando aparecieron problemas y cómo se solventaron. Tras ello, se hacen simulaciones a diferentes ángulos de ataque y en condiciones de vuelo sub y supersónico, correspondiéndose con los diferentes regímenes de vuelo en despegue y crucero, respectivamente. Tras esto, se estudia la variación con respecto al ángulo de ataque de los coeficientes de sustentación, resistencia y momentos para cada régimen de vuelo, junto con cualquier otro dato que fuera útil para comprender y validar los resultados obtenidos y cualquier anormalidad hallada. El siguiente paso tomado fue la validación de todos los resultados obtenidos, logrado contrastándolos con la teoría referida a las alas delta y datos bibliográficos del rendimiento aerodinámico del Concorde.

Por último, se hacen una discusión del presupuesto necesitado para llevar a cabo éste proyecto y su relación con los Objetivos de Desarrollo Sostenible de la ONU, seguidos de una conclusión para cerrar el documento.

1 Nomenclature and Symbol Index (first greek, then latin letters)

Variable	Description	Units
γ	Specific heat ratio	-
μ_C	Air Viscosity at Cruise altitude	$Pa \cdot s$
μ_{TO}	Air Viscosity at Take-off altitude	$Pa \cdot s$
ρ	Air Density	kg/m^3
ρ_C	Air Density at Cruise altitude	kg/m^3
ρ_{TO}	Air Density at Take-off altitude	kg/m^3
AE	Aerodynamic Efficiency (lift to drag ratio)	-
$AE_{C,max}$	Maximum Aerodynamic Efficiency (lift to drag ratio) in cruise conditions	-
a_C	Speed of Sound at Cruise altitude	m/s
a_{TO}	Speed of Sound at Take-off altitude	m/s
b	Aircraft Wingspan	m
C_D	Drag coefficient	-
C_L	Lift coefficient	-
C_M	Pitch moment coefficient	-
c_r	Wing chord at its root	m
D	Drag	N
H	Aircraft Height (without landing gear)	m
h_b	Box height from the wingroot's mean line	m
h_C	Cruise altitude	m
h_{TO}	Take-off altitude	m
L	Lift	N
L_F	Aircraft Fuselage length	m
$L_{u,b}$	Box upstream length from the wingroot's leading edge	m
$L_{d,b}$	Box downstream length from the wingroot's leading edge	m
M	Pitch Moment	$N \cdot m$
M_C	Mach number in Cruise	-
M_{TO}	Mach number in Take-off	-
P_C	Air Pressure at Cruise altitude	Pa
P_{TO}	Air Pressure at Take-off altitude	Pa
R	Ideal gas constant	$J/(kg \cdot K)$
Re	Reynolds number	-
S	Wing surface area	m^2
T_C	Air Temperature at Cruise altitude	K
T_{TO}	Air Temperature at Take-off altitude	K
v	Airspeed	m/s
v_C	Cruise airspeed	m/s
v_{TO}	Take-off airspeed	m/s
w_b	Box width from the wing's symmetry plane	m

2 Introduction

Supersonic flight has always been an attractive concept for long-range travel, since it allows to cover vast distances in shorter periods of time than what is currently possible, as all passenger aircraft nowadays fly at speeds below Mach 1. One of the only exceptions to this rule was the aircraft known as the Concorde.

The Aéroespatiale-BAC Concorde started development in 1962 as a joint British and French venture to design and manufacture a long-range supersonic aircraft for commercial purposes. The main reasons for this cooperation were the desire to share costs and risks between both countries (who the were the main financiers of the project), and it was this accord that resulted in the aircraft being named "Concorde" ("Concord" in English).

The first aircraft started entering service in 1976 (seven years after its first flight), and allowed for supersonic travel between cities such as New York and London, which was one of the main routes covered by it. As a matter of fact, the high speeds that could be achieved by the Concorde meant that the flight could be completed in around 3 hours, which is noticeably less than what it takes to cover that same route with modern aircraft nowadays (around 8 hours).

Despite this, the Concorde proved extremely costly to design, develop, manufacture and maintain, meaning that it was never made profitable through its almost 30 year long career. This, together with the infamous accident of 25 July 2000, which resulted in the deaths of 113 people, ended up leading to the retirement of the aircraft by 2003, with only 14 of them having taken to the skies. [1]

In the end, the Concorde was one of only two supersonic commercial aircraft designs that was ever realized and saw service, being a noticeably milestone in commercial aviation development.

Nonetheless, with the development of the aeronautical sector and the growing demand to be able to travel as fast as possible, several concepts and technical demonstrators have appeared to explore the possibility of, once again, transporting passengers at super (or even hyper) sonic speeds.

This, together with the desire of the author of this Thesis to better understand the behaviour of delta-shaped wings under different flight regimes and how to work with Computational Fluid Dynamics (CFD) tools, made the Concorde a very suitable choice to base this Thesis around.

Therefore, a study of the aerodynamic behaviour of the Concorde and, more specifically, its delta-shaped wing, is performed and explained throughout this document, with the intent that performing this study with a CFD tool such as the software Star-CCM+ would allow the student writing this Thesis to deepen his knowledge in using said tools.

3 Flight Conditions and Dimensions

First of all, it was necessary to determine the main dimensions of relevance of the Concorde, some of which were used to then dimension some aspects of the CFD study, or to calculate the values of some relevant variables. Therefore, the most important ones are presented in the following table:

Variable	Value	Variable	Value	Variable	Value
L_F (m)	62.10	b (m)	25.50	H (m)	11.30
c_r (m)	29.29	S (m^2)	359.0	-	-

Table 1: Table with the main dimensions of the Concorde.[2]

Then, for the purposes of this project, it was necessary to establish the flight conditions which were to be studied. Since it was desired to evaluate the aerodynamics of the Concorde at sub and supersonic speeds, it was decided to consider that the aircraft was in take off and cruise conditions, respectively. As such, the flight conditions are as follows:

Variable	Value	Variable	Value
h_{TO} (m)	0.000	h_C (m)	17'000
v_{TO} (m/s)	111.11	v_C (m/s)	600.00
P_{TO} (Pa)	101'325	P_C (Pa)	8'786.68
T_{TO} (K)	288.15	T_C (K)	216.65
ρ_{TO} (kg/m^3)	1.225	ρ_C (kg/m^3)	0.141
μ_{TO} $(Pa \cdot s)$	1.812 E-5	μ_C $(Pa \cdot s)$	1.432 E-5
a_{TO} (m/s)	340.294	a_C (m/s)	295.070
M_{TO} (-)	0.327	M_C (-)	2.033

Table 2: Table with the flight conditions for the Concorde at Take-Off (subscript "TO") and Cruise (subscript "C").[3],[4],[5]

It should be noted that, in both flight conditions, the same wing geometry is used. That is, at no point are flap or elevon deflection considered, while the landing gear is always assumed to be retracted. Having discussed all of this, it was then possible to move on to everything related with the preparation and execution of the CFD study.

4 CFD Study Pre-processing

The process followed to be able to perform the CFD study included taking a 3D model and simplifying it, importing it into Star-CCM+, and then making a convergence and mesh independence study.

4.a Procurement of 3D Model

The first step in the process was, as stated, to procure a 3D model of the Concorde which was relatively simple and, then, further simplifying it to obtain one that would allow to perform calculations in CFD without a need to reduce the size of the model, making too big or complex meshes, or making too many iterations. As such, a CAD model was downloaded from the GrabCad website and is shown here:

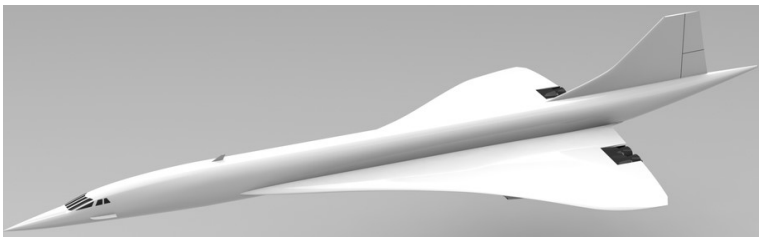

Figure 1: Isometric view of the 3D model used as the starting point for the study. [6]

One this model was downloaded, the following simplifications were performed:

- The fuselage and vertical stabilizer were completely removed, since the object of the study was to analyze the aerodynamics of a delta-shaped wing like that of the Concorde.
- The engines were likewise eliminated, as the performed study equates to putting the aircraft in a wind tunnel, so the engines themselves do not provide anything to the study other than complexity.
- Even if it might constitute an oversimplification, the engine nacelles were also removed, as calculating the behaviour of the flow going through them might over-complicate a problem that, in and of itself, would be quite hard to compute.

The result of all the performed simplifications listed above can be appreciated in Figure 2a.

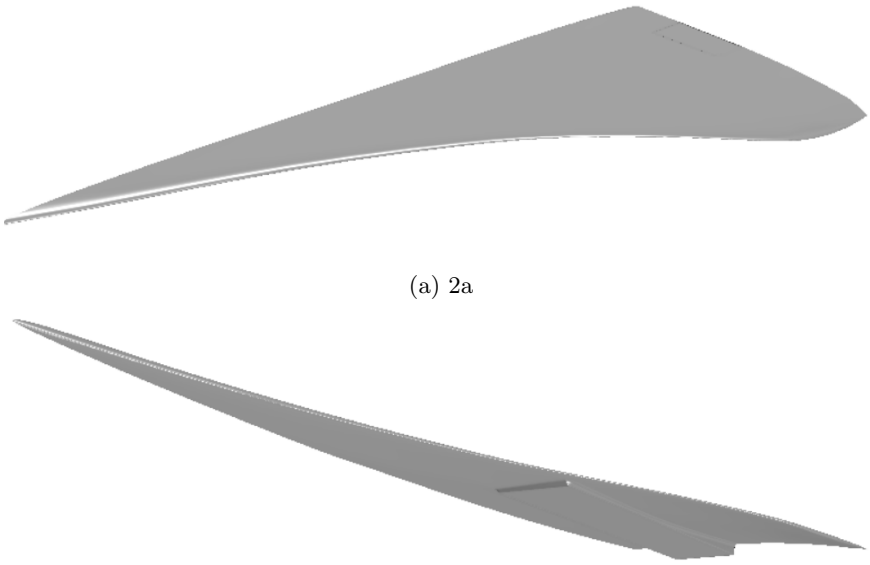

(a) 2a

(b) 2b

Figure 2: (from top to bottom) Isometric view of the simplified 3D model of the extrados and of the intrados (respectively) of the wing used to perform the study.

It should be noted that some of these decisions were taken in an attempt to make the problem as simple as possible to calculate, since the student's computer was used to perform the CFD study and, as such, the complexity of the problem would be limited to what could be calculated. Nonetheless, it should also be remarked that the 3D model retained the original dimensions of the Concorde instead of it being made to scale in an attempt to simplify the problem. This was a deliberate choice, since reducing the size of the wing would require that, if possible, both the Reynolds and Mach numbers are the same for both the model and the real aircraft. These are given by the following relations:

$$Re = \frac{\rho \cdot v \cdot L_c}{\mu} \qquad M = \frac{v}{a} \qquad a = \sqrt{\gamma \cdot R \cdot T} \tag{1}$$

If one studies these relations, it is then clear to see that, in order to maintain the value of the Reynolds number (while not changing the atmospheric properties), if the characteristic length (L_c) is reduced, the flow's velocity has to be increased. Since it is desired to avoid having trans-sonic (or hyper-sonic) flight conditions, it should be noted that increasing too much the velocity would not be advisable. Therefore, to avoid any kind of issue related to this, it was decided to maintain the original size of the wing, admitting thus that the results may not be entirely accurate because it is probable that the mesh required to attain mesh independence and, therefore, valid data, would have too many elements to be solved in a timely manner without using a more powerful computer.

4.b Meshing

Having obtained and simplified the 3D model to be used in the CFD study, it was then necessary to discuss the mesh used and the dimensions of the domain to be meshed. Said domain consisted of two parts:

- An outer box, with a semicircular part upstream of the leading edge of the wing (at its root), where the mesh is relatively coarse.
- An inner trapezoidal box where the mesh will be refined close to the wing to obtain a greater accuracy when solving the behaviour of the flow close to the wing and in its wake.

The dimensions of both of these regions to be meshed are presented in the following table and are (mostly) expressed with respect to the wing's root chord:

	Outer Box		Inner Box	
$L_{u,b}\ (m)$	$5 \cdot c_r$	146.4	$\frac{c_r}{2}$	14.64
$L_{d,b}\ (m)$	$8 \cdot c_r$	234.3	$3 \cdot c_r$	87.87
$h_b\ (m)$	$5 \cdot c_r$	146.4	-	15.00
$w_b\ (m)$	$3 \cdot \frac{b}{2}$	38.25	-	15.00

Table 3: Table the with main dimensions of the regions used to mesh the 3D model.

All of this leads to the domain to be meshed having the shape presented in the following figures:

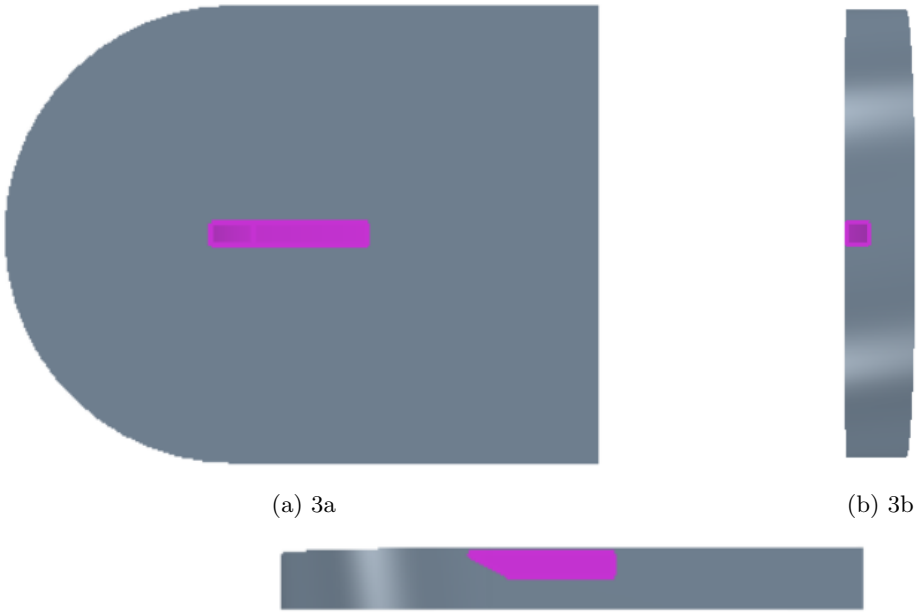

(a) 3a

(b) 3b

(c) 3c

Figure 3: (from left to right and top to bottom) Profile, front and top views of the domain to be meshed, with the outer box in grey and the inner box in pink, respectively.

With this in mind, it was then necessary to decide on the type of mesh to be used and the main parameters defining it. Regarding the former, it was chosen to use the same mesh for all cases, since this would simplify a lot the mesh validation and simulation process, although some issues regarding accuracy may arise from this. Said mesh would be made using a Polyhedral Mesher, due to its ability to mesh complex contours with relatively few elements, in conjunction with a Thin Mesher and Surface Remesher, to allow for a finer mesh near the body and avoid any meshing issues that might have occurred due to the shape of the wing.

An attempt was made to use a Prism Layer Mesher, to be able to more accurately model the boundary layer over the wing, but this was not possible, since the shape of the wing, specially near the leading and trailing edges, did not allow for a reasonably-shaped prism layer.

Having chosen the meshers to be used, most of its parameters were left in their preset values, with the exception of the ones that were set to the ones below, some of which were based on the studied bibliography:

Variable	Value
Base size (m)	0.8
Volume Growth Rate (-)	1.2
Minimum Surface Size (%)	10

Table 4: Table with the main parameters that were modified when defining the mesh.[7] [8] [9] [10]

Regarding Volume Growth Rate, it should be pointed out that a smaller value of 1.1 might be advisable to obtain a mesh that is small enough to allow for accurate calculations to take place. Nonetheless, this would result in a mesh with too many elements to be solvable in a reasonable ammount of time for all cases of study.

In addition to this, in the Inner Box, a custom base size of 7.5 % (0.06 m) was set to refine the mesh close to the wing and, thus, obtain more accurate results. The aforementioned values were chosen because, in the end, they yielded a mesh with a reasonable number of elements (around 1.8 million) that would thus allow to perform simulations in a timely manner. The resulting mesh is presented in Figures 4a and 4b.

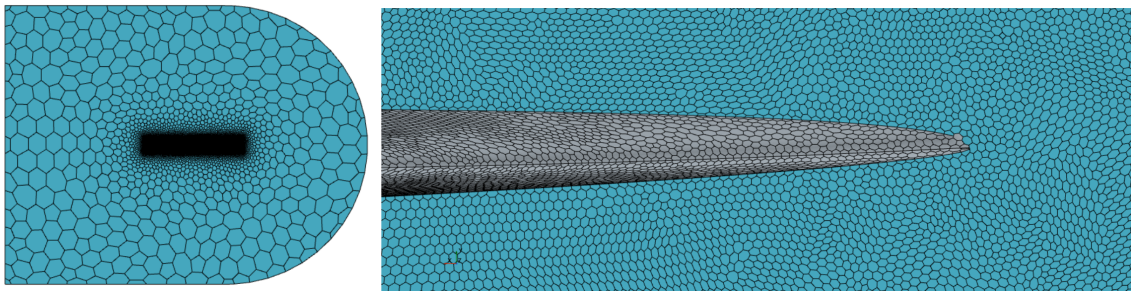

(a) 4a (b) 4b

Figure 4: (from left to right) Side view from the symmetry plane of the obtained mesh with the parameters described in Table 4 (upstream side to the right of both pictures) for the general mesh, and a close up of the wing's leading edge, respectively.

It should be noted that more refined meshes could be obtained and would thus yield more accurate results. However, this would have led to very long simulation times, and since it was needed to take into account the limited time for the realisation of this project, the presented mesh is taken. Nonetheless, a proper mesh independence analysis was also performed to make sure that the chosen mesh provided accurate results and, if it did not, that a finer one would be required.

In any case, once the mesh had been made, the following boundaries were assigned to each of the region's surfaces:

- The upstream (curved) surface of the domain, lower surface and the outer-side surface were set to be velocity inlets or free-stream boundaries if the case of study was the take-off (subsonic) or cruise (supersonic) one, respectively.
- The downstream surface was set to be a pressure outlet.
- The symmetry plane was set to be a symmetry boundary condition, thus allowing for the use of half the wing for the calculations.
- The upper surface of the domain was set to be a velocity inlet or free-stream boundary condition (for sub or supersonic calculations, respectively), when the angle of attack of the flow was of 0°, and a pressure outlet for any other case. This choice was made because it was observed that swtiching from velocity inlet (or free-stream) to pressure outlet allowed for faster convergence.

Having discussed all of the aspects related to the domain's meshing, it was then possible to move on to the definition of all of the different solvers used in each case.

4.c CFD Model and Solver Set Up

Regarding the models that the CFD software was to use when performing the corresponding calculations, we have to distinguish between those that were common for both take-off (subsonic) and cruise (supersonic) conditions, and the ones that were specific for each of them. Starting with the former ones, these are:

- **Steady flow**, since we assumed that the aircraft is maintaining constant velocity in both flight regimes.
- **Ideal gas**, since this can generally be assumed for air without leading to a great error.
- **Turbulent flow**, as we expect the air to be noticeably perturbed by the presence of the wing, specially at higher angles of attack, therefore leading to very high Reynolds numbers (2.2 E+8 and 1.7 E+8 for subsonic and supersonic conditions, respectively). Since the usual limit to start considering turbulent flow for external aerodynamics is given by a Reynolds number of 2 E+5, this assumption can be considered to be correct. [11]
- Because of the previous reason, and taking into account that we are mainly performing aerodynamics-related calculations, we use the **Spalart-Allmaras turbulence model** which is quite accurate for this purpose, being its main limitation not being able to solve with enough accuracy the turbulence conditions that lead to a stall, specially detached flow. This however is not the aim of this project, so the indicated model is considered to be sufficient. Additionally, it was also chosen because, of the consulted bibliography, many academic works used it or recommended its use for aerodynamic applications. [7], [8], [12], [13], [14], [15], [16], [17]
- **Three Dimensional flow**, since we are solving for a three dimensional domain.
- **Newtonian fluid**, as all the simulations are being made in air, which is a notoriously Newtonian fluid.

Regarding the specific considerations made for the study in take-off conditions (subsonic flight), we remark that a **Segregated** solver was used, since the Mach number of the flow is approximately 0.3, as seen in Table 3, thus allowing to consider incompressible flow. On the other hand, for cruise (supersonic) conditions, this no longer applies and, as such, compressible flow must be considered, so a **Coupled** solver was used instead.[18]

Once these lasts aspects were decided upon and the simulation files were all meshed and set, it was then possible to move on and start with the calculations of all of the different cases of study.

5 Convergence and Mesh Independence Studies

5.a Convergence Study

Regarding the evaluation of the convergence of the simulations, the main criteria used here was that the values of the residuals at the end of the calculations had to be (at the very least) below 10^{-3}. This might seem relatively lax , since it is common to take as convergence criterion that the residuals ought to be smaller than 10^{-6} for all of the equations except for continuity, for which 10^{-3} is considered to be acceptable. However, the one described here is used due to the fact that it is expected that the mesh coarseness and the size of the domain might make it very hard to get the values corresponding to the latter, stricter, criterion. [19]

In addition to the values of the residuals, the convergence of the simulations would also be assessed based on the variation between iterations of the main parameters to be studied (drag, lift and pitch moment coefficients). Said criterion consisted on ensuring that the aforementioned variation was below 0.1%, since this would mean that the simulations had reached a final value for these coefficients and would not change from it. It should also be noted that these parameters are defined (and calculated by the CFD software) as follows:

$$C_L = \frac{L}{\frac{1}{2} \cdot \rho \cdot v^2 \cdot S} \qquad C_D = \frac{D}{\frac{1}{2} \cdot \rho \cdot v^2 \cdot S} \qquad C_M = \frac{M}{\frac{1}{2} \cdot \rho \cdot v^2 \cdot S \cdot c_r} \tag{2}$$

Where the lift and drag forces are defined as the forces acting in the direction perpendicular and parallel to the flow, respectively, while the pitch moment is the moment that appears in the axis that follows the wingspan.

On a more general note, to perform the studies to obtain the polar curves, the simulations were all started at angles of attack of 0^{o} and this value was increased in intervals of 4^{o} to ensure that results were representative and there were not too many simulations to be performed. It should also be explained that the variation of the angle of attack was attained by rotating a coordinate system and, thus, the direction of the flow's velocity, since this would allow to (in theory) use the same exact mesh and domain for all cases. [20], [21]

Once they were started and their results studied for both sub and supersonic flight, convergence was observed in only a handful of cases, being all of them subsonic cases of study at low angles of attack (12 degrees and lower). This was caused due to different issues and resulted in different residuals not converging at all.

If we study the plots of the residuals for both sub and supersonic flight conditions, we can observe several problems. If we start with the former of the two cases, we observe that, up to 16^{o}, convergence was attained, but, at this angle of attack, the following graph is obtained:

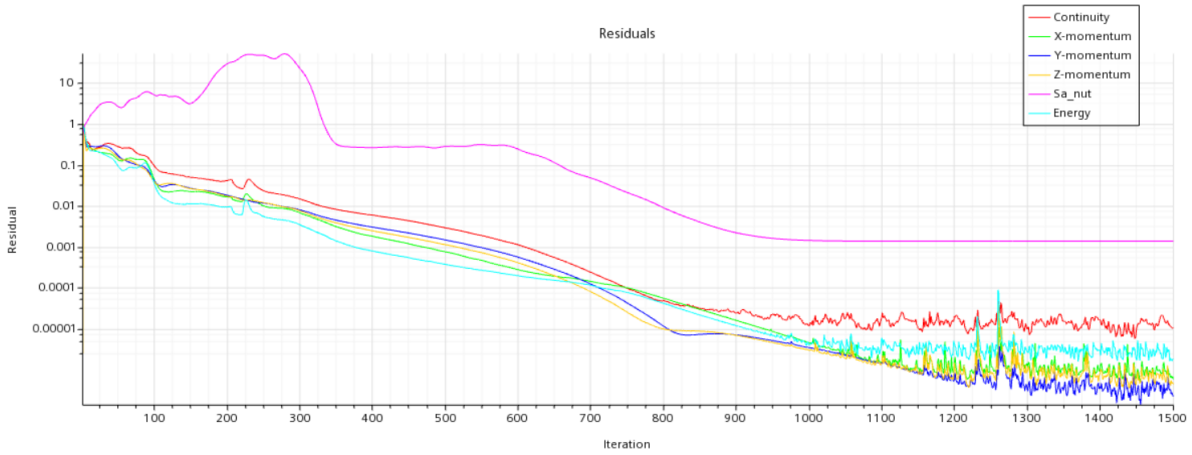

Figure 5: Graph representing the values of the residuals for an angle of attack of 16^{o} and subsonic flight conditions.

As it can be clearly observed in Figure 5, all residuals do converge after several iterations, but this does not occur with the ones referred to the turbulent model. This could perhaps be caused by the fact that the wing presented stall conditions at some point of the wingspan.

This, however, was considered to be unlikely, since it is widely-known that delta-shaped wings such as the one being studied have a high stall angle of attack, since they require quite high incidences to be able to maintain flight. [22] Additionally, if stall conditions were in fact occurring and causing problems with convergence, it would be reasonable to expect that at least other residuals presented this same issue.

Nonetheless, studying the residuals for cruising conditions, allowed to ascertain which might be the cause behind the convergence issues. For this second case, the residuals did not converge at all even for a zero degree angle of attack (except the one of the turbulent model), as it can be seen in Figure 6:

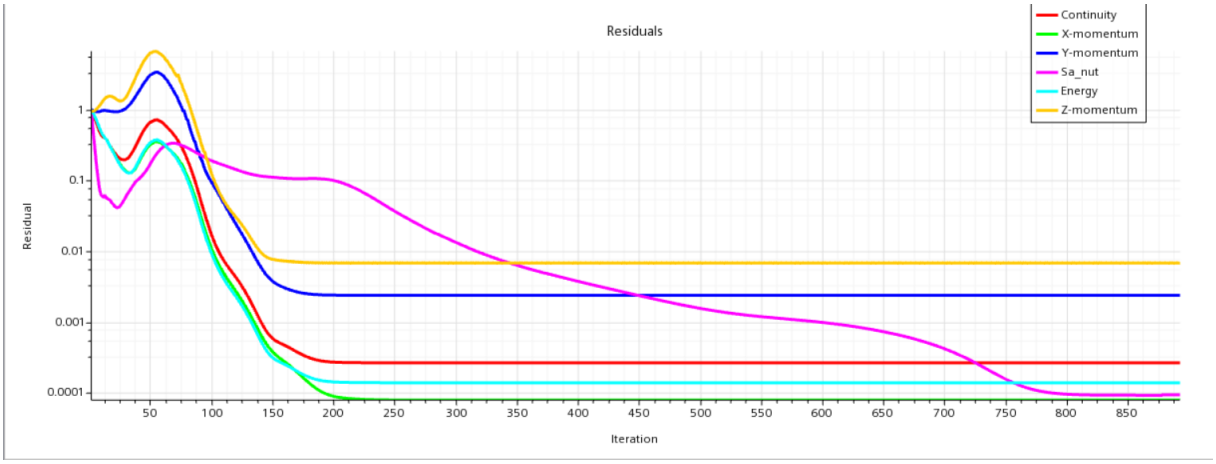

Figure 6: Graph representing the values of the residuals for an angle of attack of 0º and supersonic flight conditions.

Together with this, it was observed that, for several iterations of the simulations in both cases, but specially in cruise conditions, the minimum value of the Absolute Pressure was being limited in several cells.

Therefore, it was concluded that the complexity of the calculations being performed, together with the limitations being imposed by the coarseness of the mesh, were the main cause of the convergence problems being observed. Hence, the following simplifications were introduced to both sub and supersonic cases in an attempt to simplify the calculation process:

- The gradient's Custom Accuracy Level was set from 2 to 1.
- The turbulent's model Convection Order was set from second to first.
- The Minimum Allowable Absolute Pressure was set from 1000 Pascals to 0 Pa, so that the solution achieved convergence naturally, instead of being forced by such limits.

Specifically for supersonic conditions, the following modifications were also introduced:

- The air's dynamic viscosity was set to be governed by Sutherland's Law instead of being constant. This should only influence the dynamic viscosity in a significant manner in supersonic flight, since it establishes that the dynamic viscosity depends on the value of the flow's absolute temperature. [23]
- The coupled flow's discretization was set from second to first order.
- The coupled energy's enthalpy formulation was toggled on and flow boundary diffusion was toggled off.
- The coupled flow was set from coupled inviscid to AUSM+. The Advection Upstream Splitting Method (AUSM+) allows for a much more precise evaluation of shock-discontinuity, such as the one that appears when a shock-wave forms. [24]

These allowed to finally obtain converged results in all cases. It should be noted that these modifications were applied to all of the supersonic cases, since none of them converged, but only some of the subsonic ones, since convergence at low angles of attack was still attained.

Additionally, although for subsonic conditions it was possible to simulate until stall conditions were observed, this was not the case for supersonic conditions, where convergence was not achieved for angles of attack greater than or equal to 28º, even if all or some of the explained modifications were applied. To try and solve this, the maximum allowable temperature was also increased, but none of these allowed to attain convergence. Most probably, this issue was caused due to problems with the used 3D CAD, since it was simplified by the author of this thesis, and/or the coarseness of the used mesh.

Nothing is noted here regarding the aerodynamic coefficients, since their variation with respect to the iterations was observed to stabilise rather quickly, thus showing convergence even before this occurred for the residuals.

Having explained all of this, it is then possible to move on and start discussing everything related with the Mesh Independence Study.

5.b Mesh Independence Study

Regarding the evaluation of the mesh independence, it should be explained that, due to the amount of simulations being performed at different angles of attack, and also because of the limited time at hand, a "conventional" mesh independence study could not be performed. In this context, "conventional" is understood as refining the mesh for each and every one of the cases being simulated until the variation of the results being obtained for the lift, drag and pitch moment coefficients is below a certain threshold.

Instead, since the mesh is not modified at all between cases, it was considered that doing the mesh independence study could be performed in a single "representative" case for both subsonic and supersonic conditions. For the purposes of this study, the representative case was considered to be the one at an angle of attack of 20^{o}, since it is far enough from both the zero incidence and stall cases, and the aim would be to attain variations of less than 1% between cases for the lift, drag and pitch moment coefficient values.

Additionally, it should be pointed out that refining the mesh in a manner that would allow to attain mesh independence could result in meshes with so many elements that they could not be solved in a timely manner. As a general rule, it was considered that it was needed to increase the number of elements in each direction by at least 50% so, since we are using a 3D mesh, the overall number of elements is multiplied by a factor of 3.4 (1.5^3 since we increase the number of elements by 50% in all three directions).[25]

Therefore, should we attempt to obtain mesh independence as indicated, if one takes into account that the original mesh used had a number of around 1.8 million elements, the new mesh that should be made should have around 6.1 million elements, which might still be within what could be calculated by the computer being used. Nonetheless, it should be taken into account that, should this mesh not show that mesh independence is achieved, another, finer, mesh should be made from this one to then prove that mesh independence is indeed attained. If, by any chance, the 6.1 million element mesh proved to be the one were this is achieved, all files would then have to be simulated with this latter one, but only if the aforementioned time constraints allowed for this. This increase in number of elements was achieved by reducing the base size from 0.8 m to 0.46 m.

Since this method could very quickly lead to meshes so large that they could not be solved in a timely manner, another criterion for mesh independence was chosen to see which of the two methods worked best. This more "relaxed" approach consisted in attempting to increase the number of elements by a factor of 1.5, but overall, instead of in every direction. This would mean that, from the original 1.8 million element mesh, another one with around 2.7 million elements would be made to check for mesh independence. [26]

In this second case, only the base size in the inner box of the domain (see Figures 3a to 3c) was reduced from 7.5% to 6.2% the base size of the mesh elements, since this would be where the difference in the obtained results would be made when reducing base element size.

Before even discussing the variation of the results of these two meshes with respect to the original case, it should be remarked that the original one was not very good. This was due to all of the compromises that had been previously made and that have been already explained. For example, the lack of a prism layer when meshing resulted in the boundary layer presenting an irregular shape at some points of the wing that affected the flow around it, as it can be clearly seen in the following figures:

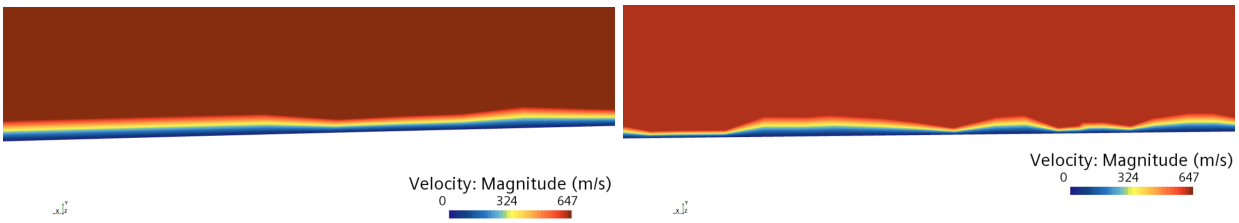

(a) 7a (b) 7b

Figure 7: (from left to right) Close-up of a velocity scene showing the irregularities in the shape of the boundary layer close to the trailing edge at both the symmetry plane of the wing and at an intermediate section at 3 m from the symmetry plane (respectively) for supersonic flight conditions and an angle of attack of 20º.

This issue was most probably being caused by the fact that a mesh with irregular elements was being used. The most obvious solution to this would be to use regular mesh elements near the wing to be able to properly model the boundary layer.

This could be achieved by either using a Tetrahedral Mesher instead of the Polyhedral one being used. However, the former led to a mesh with too many elements to be able to compute any solution to this problem. To put an example, both a Tetrahedral and Polyhedral meshes were made for the same exact domain and element dimensions, volume growth rate, element refinement near the body and etcetera when the mesh parameters were still being decided on. The resulting meshes had around 15 and 0.2 million elements, respectively. This shows that, should a tetrahedral mesh be used to have more regular elements around the wing, the overall mesh parameters would have to be modified to allow for a mesh that could be solved in a timely manner.

On the other hand, another possible solution to the boundary layer issue could be found by using a Prism Layer Mesher, which was done and attempted. Nonetheless, as it was indicated in Section 4.b, the result was a mesh that only presented a prism mesh around the wing over most of the extrados and intrados, with the leading and trailing edges not presenting a reasonably shaped one due to its shape, as it can be observed in Figure 8. This, lead to some uncertainty on how the Polyhedral Mesh and the cells of the prism layer would interact and how this could affect the solution, specially in supersonic flight conditions. It should be noted that the addition of the prism layer increased the number of elements of the mesh to around 2.3 million elements and that refining the overall base size of the elements from 0.8 m to 0.46 m did not seem to solve this issue entirely, meaning that very small base sizes (at least in the Inner Box of the domain) would be required to properly model the boundary layer, which could lead to quite fine meshes and, thus, long simulation times.

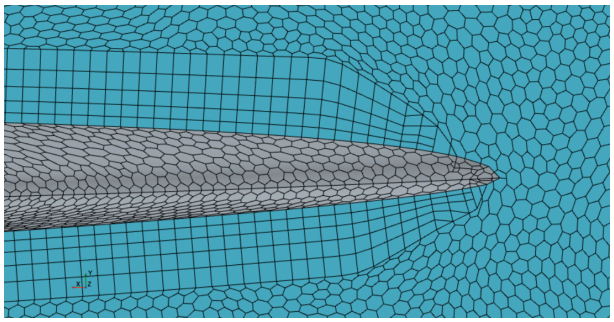

Figure 8: Close up of a mesh scene on the symmetry plane of the wing at the leading edge showing the irregular shape of the prism layer formed (with the upstream of the flow being to the right of the image).

In any case, all three of these possible solutions (increasing the number of elements by 3.4, by 1.5 and adding a prism layer) were attempted, and the variations of the obtained results with respect to the original mesh were all logged and are presented in Table 5. It should also be pointed out that the first of the three cases needed around 11 hours of simulating to be able to converge for the subsonic case, which would lead to the conclusion that the supersonic cases could take even longer (as they would be much harder to compute).

This could allow us to conclude that this mesh takes to much time to calculate a single case to be able to use it in a widespread manner for all cases.

	Subsonic Conditions at 20º		
Mesh	C_L Variation (%)	C_D Variation (%)	C_M Variation (%)
3.4x Increase (T11B4)	0.85	0.38	0.73
1.5x Increase (T11A2)	0.30	0.14	0.30
Prism Layer Addition (T13)	3.27	4.19	3.02

Table 5: Table with the percentage variations of the aerodynamic coefficients for the different meshes that were made to test mesh independence with respect to the results of the original mesh as described in Section 4.b for subsonic flight conditions and an angle of attack of 20º.

The evaluation of the results in Table 5 allows to see that, according to any of the two considered criteria, mesh independence had already been attained with the original mesh used. However, the evaluation of the results provided by the addition of the Prism Layer Mesher without modifying any other of the mesh's parameters, allows to see that mesh independence had not in fact been attained, being the main factor behind this the fact that the boundary layer was not being properly modelled. We can check if this is the case by comparing (as a representative example) Figures 9a and 9b:

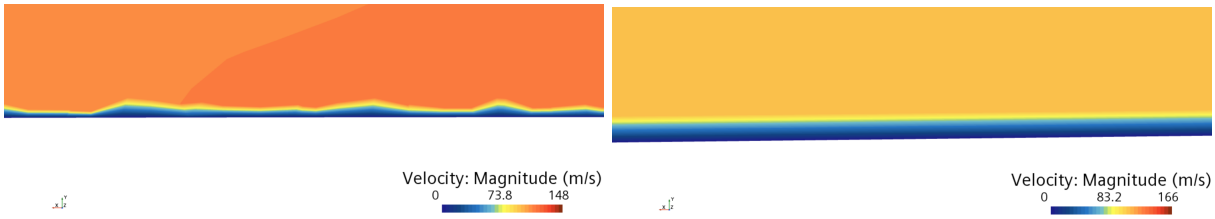

(a) 9a (b) 9b

Figure 9: (from left to right) Close-up of a velocity scene showing the shape of the boundary layer over the wing's extrados at the symmetry plane in subsonic flight conditions at an angle of attack of 20º without and with a Prism Layer Mesher (respectively).

As it can be clearly seen, the addition of the Prism Layer Mesher allows to obtain a boundary layer with a shape that is much smoother and, as such, corresponds more with what could be expected to happen in real life. It should also be pointed out that these figures allow to see, when compared to Figures 7a and 7b, that this issue is not one exclussive to the supersonic case, but rather one that is common to all simulation files.

Therefore, starting from this second mesh, an attempt was made to attain mesh independence, since it would seem that the proper modelling of part of the boundary layer and mesh refinement would allow to attain mesh independence or, at the very least, more accurate results. Once again, a similar approach to the previous one was taken, that is, increasing the number of elements by 3.4 through a simple base size reduction from 0.8 m to 0.46 m, which lead to a mesh of approximately 7.4 million elements (as opposed to the almost 7.7 million to be obtained) and variations in the coefficients of 0.30% at most when comparing to the case with just the prism layer added. This showed that, theoretically, mesh independence had in fact been achieved, without needing to attempt to increase the number of elements just by 1.5, since the variation in the results would be expected to be smaller. Nonetheless, it should be pointed out that, should the 3D model be refined further (or made to have a smoother overall surface from the get go), the prism layer could have been extended to the overall wing surface, thus allowing for an even more accurate boundary layer modelling.

To make sure that the obtained results were not case-specific, an identical process was followed for supersonic conditions and the same angle of attack, being the obtained results presented in Table 6.

	Supersonic Conditions at 20º		
Mesh	C_L Variation (%)	C_D Variation (%)	C_M Variation (%)
1.5x Increase (T11A2)	- 0.09	- 0.18	-0.07
Prism Layer Addition (T13)	- 0.04	- 0.30	- 0.04

Table 6: Table with the percentage variations of the aerodynamic coefficients for the different meshes that were made to test mesh independence with respect to the results of the original mesh as described in Section 4.b for supersonic flight conditions and an angle of attack of 20º.

In the supersonic case, as it can be seen, neither the mesh refinement using a factor of 1.5 nor the addition of a prism layer contributed to the results presenting variations over 1% in absolute value. It should be pointed out that performing calculations for meshes refined by a factor of 3.4 for the cases without and with prism layer was attempted, however, some problems were encountered.

The main issues that prevented the realisation of the simulation for those meshes were the fact that the used laptop started running out of memory and that the RAM memory was insufficient to perform these calculations. This, together with the fact that time was running short, lead to these cases being omitted after several attempts at doing them were frustrated due to an insufficient virtual memory error occurring or the used laptop crashing.

Even if mesh T13 (the original one used, known as T11, with a Prism Layer Mesher added) presented mesh independence characteristics and did not take too much time to run when compared to the original used mesh (at least in subsonic flight conditions, since in the supersonic case this could not be properly assessed), all of the results that are presented in the following sections are taken from simulations being performed for the original mesh as described in Section 4.b. This was done because the boundary layer was not being properly modelled around the leading edge by the Prism Layer Mesher and due to the aforementioned lack of time.

6 Study and Validation of Results

6.a Observed Results

Once convergence was attained and the mesh independence study was concluded, it was then possible to move on and evaluate the obtained results, as well as trying to determine their validity with respect to real life aerodynamic performance data of the Concorde.

Having performed simulations for angles of attack ranging from 0º to 30º, it was then possible to obtain the values of the lift, drag and pitch moment coefficients for the different incidences.

Should one observe the lift coefficient curve for subsonic (take-off) conditions, as presented in Figure 10, it is then clear to see that stall in these flight conditions seems to start appearing at angles of attack greater than 28º, which then would allow to conclude that the resulting curve yields lower lift coefficient values than other aircraft with regular (not delta-shaped) wings, but manages to avoid stall up to greater angles of attack. On the other hand, it seems that stall conditions are not reached before (or even at) 28º in supersonic flight.

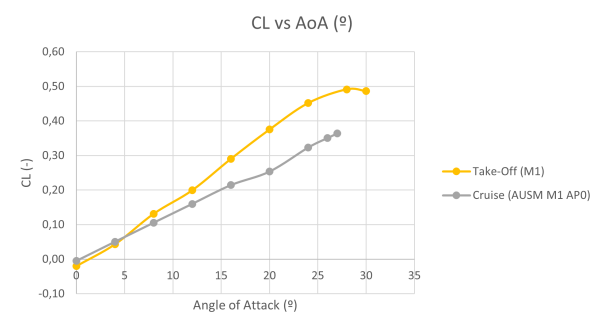

Figure 10: Graph representing the values of lift coefficient against the angle of attack for subsonic and supersonic conditions.

To make sure that stall is in fact occurring at an angle of attack of 30º for subsonic conditions, we make a velocity scene and represent it at different sections of the wing to observe whether the flow presents any regions were boundary layer detachment might be occurring or not. Thus, we can observe the following scenes:

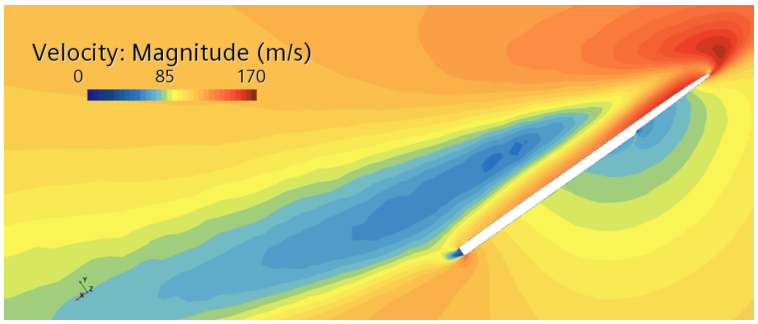

(a) 11a

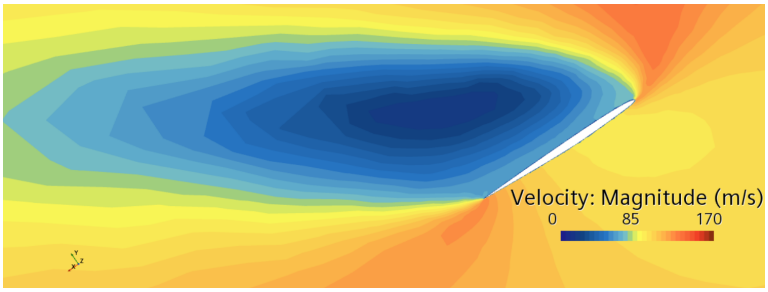

(b) 11b

Figure 11: (from top to bottom) Velocity scenes of the flow in subsonic flight conditions and an angle of attack of 30º at sections at 3 m and 10 m (respectively) from the symmetry plane of the wing (flow direction is from right to left on both of them) parallel to it.

The evaluation and comparison of Figures 11a and 11b allows to see that some stagnation of the flow occurs over the extrados at 3 m from the symmetry plane, since there is some flow slow down (as appreciated by the blue area), but the flow over it remains attached as it is still accelerated over the extrados. However, the second scene allows to conclude that the flow detaches close to the wingtips, causing the wing sections closer to them to start stalling. This detachment then extends towards the wingroot and affects the behaviour of the flow at different sections, even if the flow remains attached. The closer we move to the symmetry plane of the wing, the smaller the influence of this effect is.

In addition to all of this, there is a slight anomaly in the overall velocity scene shown in Figure 11a, were a slow down of the flow can be clearly appreciated around the end of the first third of the wing. A close up of the region in question allows to see what is causing this issue:

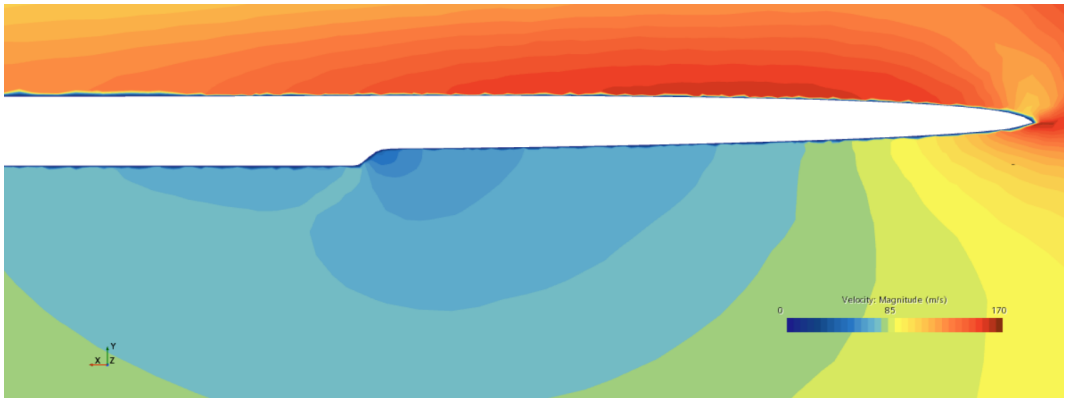

Figure 12: Close up over the leading edge of a velocity scene of the flow in subsonic flight conditions and an angle of attack of 30º at a section at 3 m from the symmetry plane of the wing (flow direction is from right to left).

The evaluation of Figure 12 allows to see how the reduction in velocity of the flow is being caused by a slight step in the wing's intrados. This corresponds to what remained of the engine's nacelles after curating the 3D model used for the simulations. It is also interesting to point out that it is working as intended, since its main purpose is to reduce the overall velocity of the flow and, therefore, increase the pressure at the engine inlet, which would in turn allow for a greater thrust being generated by the engines.

To substantiate the claim that the slope of the polar curve for the Concorde is much smaller (but takes longer to present stall) than for a conventional aircraft, we can compare the obtained curve to the plot of the linear part of the lift curve, that is, the lift curve up to the angle of attack were stall starts to occur, of the Boeing 747-200, which has a conventional wing:

Figure 13: Graph representing the values of the lift coefficient against the angle of attack (in degrees) for subsonic flight conditions for the performed CFD study on the Concorde and the Boeing 747.[27]

As it can be clearly seen by studying Figure 13, the angle of attack at which stall appears is considerably greater than the value for the 747-200, but the overall values of the coefficient are considerably smaller for the Concorde, which coincides with the idea that delta-shaped wings have a much smaller polar curve slope. This is true even if we account for the greater value that the 747 presents at 0º, which is probably caused by a geometric or aerodynamic twist, or by the fact that a non-symmetric airfoil is being used. It should also be kept in mind that other reasons might be influencing the difference in the values of the lift coefficient between the two aircraft, since factors such as the aspect ratio are not being discussed here.

The main reason behind these differences in slope and maximum angle of attack is the fact that, while a conventional wing has a wing tip where vortices form due to the differences in pressure between the intrados and extrados, a delta-shaped wing does not present a wingtip. Rather, in subsonic conditions, a peak of suction appears at the leading edge caused by the tendency of the flow to go from the intrados to the extrados. This leads to a vortex forming along the leading edge and then reattaching, which in turn

causes the appearance of a secondary vortex, thus causing the aforementioned pressure drop. This can be appreciated in Figure 14.

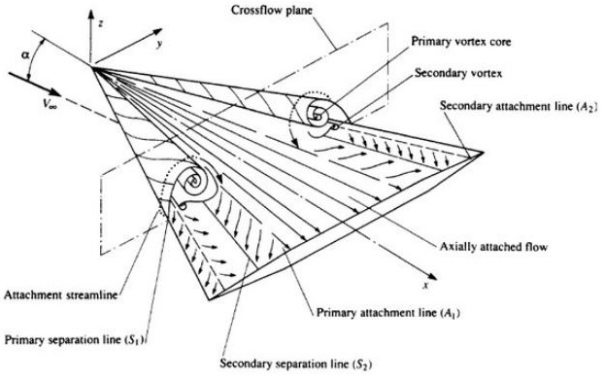

Figure 14: Drawing of the behaviour of the flow over a generic delta-shaped wing in subsonic conditions.[28]

Said vorticity over the extrados at the leading edge causes the generated lift to be greater than in supersonic conditions (were no communication between intrados and extrados exists due to the formation of a shock-wave at the leading edge or over the wing). This also means that, as it has been seen, the maximum angle of attack that can be attained before stalling is greater than in wings with a conventional shape, but also leads to a greater induced drag coefficient and, thus, greater overall drag.

Furthermore, we could also make a representation of the variation of the pressure coefficient for several sections of the wing along the X axis (in the direction of the flow) in subsonic conditions, which should allow us to appreciate the previously mentioned suction peak that occurs at the leading edge of the wing.

Figure 15: Graph representing the variation over the wingspan of the pressure coefficient at sections of the wing at 2 m, 5 m, 10 m and 20 m from the root's leading edge for subsonic flight conditions at an angle of attack of 20º.

As it can be clearly appreciated in Figure 15, the pressure coefficient stays more or less constant along the wingspan in the intrados (where possitive values are observed) and, when reaching the leading edge, a sudden drop in the pressure coefficient occurs, which causes the overall pressure coefficient distribution in the extrados to present smaller values.

Since this seems to be properly modelled in the CFD study, together with the fact that the lift curve presents a greater stall angle of attack, we could consider that part of the CFD study is being correctyl performed.

All of this also serves to explain why in supersonic flight conditions, and specially at higher angles of attack, the overall lift coefficient is noticeably smaller, since this communication between in and extrados is no longer occurring, as a shock-wave prevents the communication between intrados and extrados.

Said shockwave could be appreciated if an absolute pressure scene over the wing is represented, together with a plane section intersecting it in part and at the trailing edge, as it can be clearly seen in Figures 16a and 16b. It should be pointed out that, in both cases, different scales are used to make sure that different features to be discussed are noticeable.

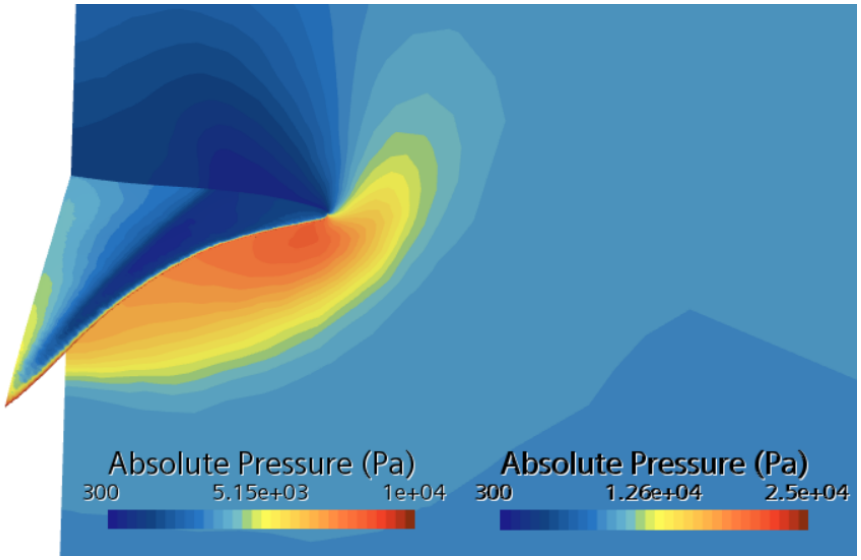

(a) 16a

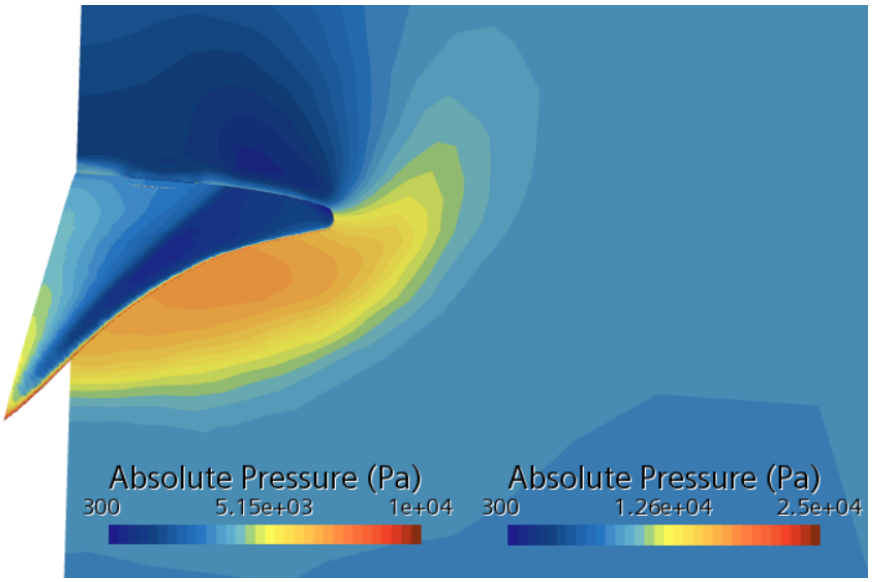

(b) 16b

Figure 16: (from top to bottom) absolute pressure scenes for the wing (left scale) and a vertical plane intersecting it at 15 m and the trailing edge, respectively (right scale).

The evaluation of Figures 16a and 16b allows to see the formation of a shockwave over the extrados of the wing, causing a sudden variation of pressure, while a bow wave appears below it. This can further be observed if the pressure coefficient at different sections of the wing along its chord is presented, as shown in Figure 17.

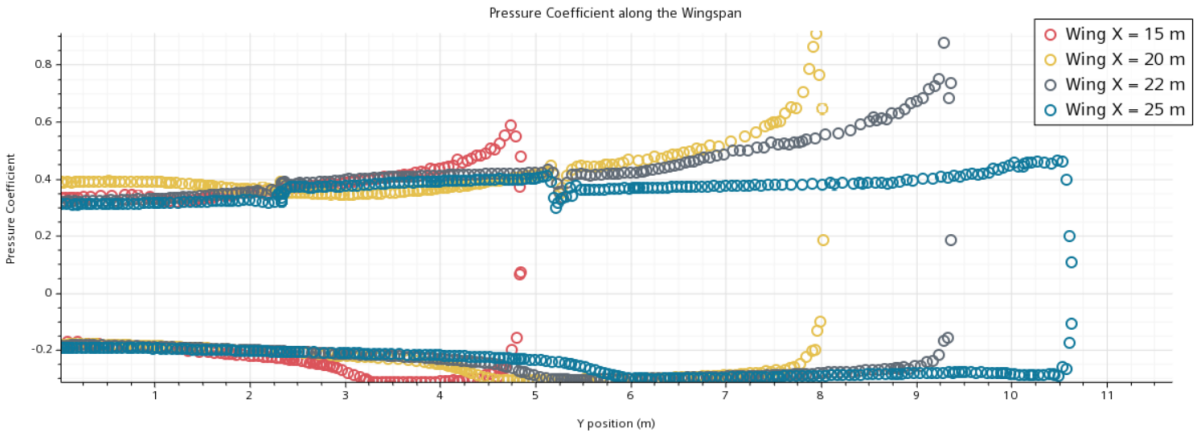

Figure 17: Graph representing the variation over the wingspan of the pressure coefficient at sections of the wing at 15 m, 20 m, 22 m and 25 m from the root's leading edge for supersonic flight conditions at an angle of attack of 20º.

The evaluation of Figure 17 allows to see how, in the sections at 20 m, 22 m and 25 m from the root's tip, a small pressure drop at around 5.2 m from the symmetry plane occurs. This would allow us to conclude that there is, as observed in Figures 16a and 16b, a weak shockwave forming over the extrados of the wing.

Continuing on with the study of the aerodynamic coefficients, should one study the drag coefficients presented in Figure 18 and compare the ones obtained for sub and supersonic conditions, it is clear to see that, because of the aforementioned reasons, the overall drag coefficient in cruise flight is smaller than the one corresponding to take-off because of the smaller induced drag coefficient, since there should not be any communication between intrados and extrados due to the presence of the shock-wave. Nonetheless, it should be noted that this difference might not be as noticeable since, even if the induced drag coefficient is made smaller, some drag also appears because of the shock-wave that forms (known as "wave drag").

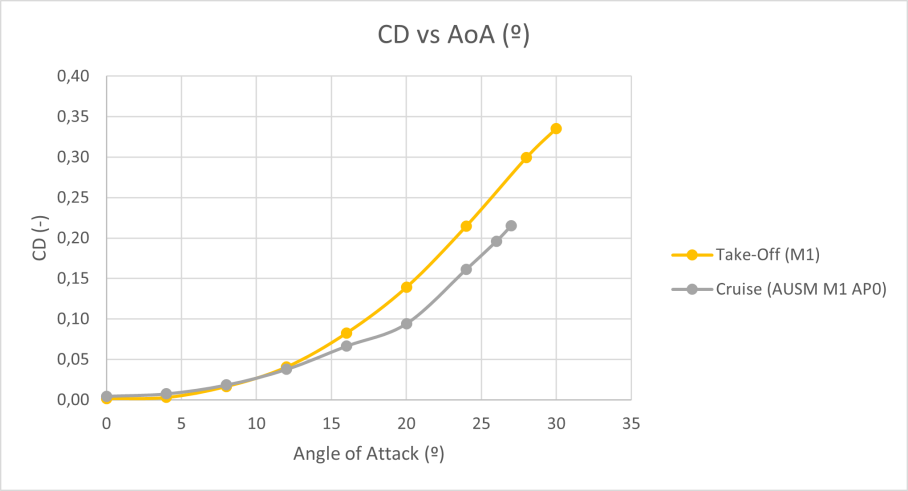

Figure 18: Graph representing the values of the drag coefficient against the angle of attack for subsonic and supersonic conditions.

The overall evaluation of the drag curve allows us to see how, as the angle of attack increases, the overall value of the drag coefficient also does in both cases, even when stall occurs in subsonic conditions at 30º (as seen in Figure 10), as the detachment of the boundary layer would lead to a decrease of the overall lift being generated, but also to an increase of the experienced drag.

We could also represent the lift-to-drag ratio (also known as Aerodynamic Efficiency), which leads to the results being shown in Figure 19.

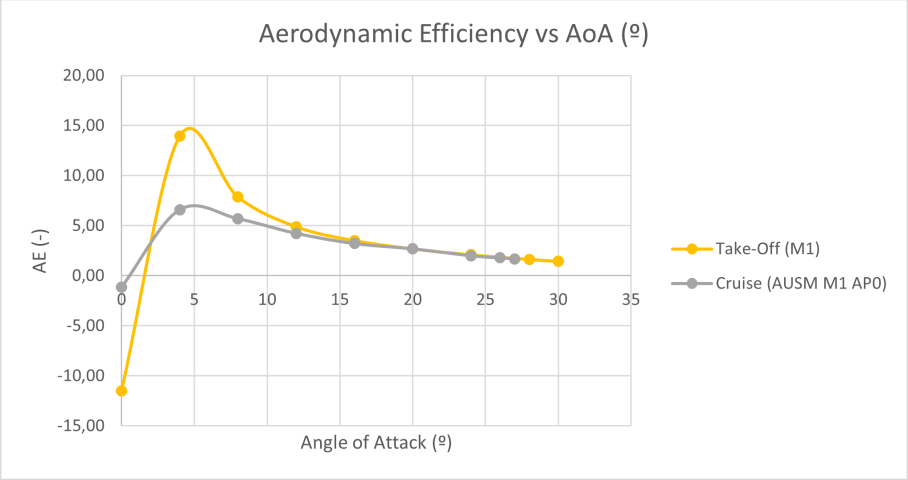

Figure 19: Graph representing the values of the aerodynamic efficiency against the angle of attack for subsonic and supersonic conditions.

The study of Figure 19 allows to see quite clearly how the overall aerodynamic efficiency at angles of attack of over 15^{o} tends to take values which are quite close between themselves for both subsonic and supersonic flight. On the other hand, for angles of attack below this value, the fact that the overall aerodynamic efficiency is noticeably larger in subsonic flight is appreciated. This is related to the already mentioned reasons regarding air flow between intrados and extrados, but also serves to illustrate that this phenomena is more advantageous regarding performance for low angles of attack when flying at subsonic speeds. The values observed at 0^{o} are not considered to be realistic (specially for subsonic flight), since they appear due to the division of a very small number by another very small number.

Last, but not least, should we represent the variation of the pitch moment coefficient with respect to the angle of attack, the tendencies seen in Figure 20 are obtained.

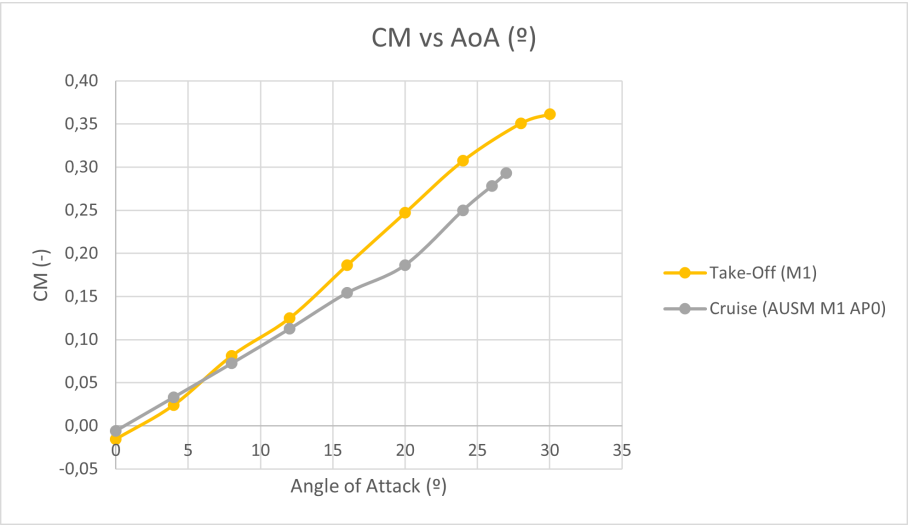

Figure 20: Graph representing the values of the pitch moment coefficient against the angle of attack for subsonic and supersonic conditions.

The evaluation of this graph allows to conclude that, for both cases, the value of the pitch moment coefficient increases as the angle of attach does, being its overall value smaller for supersonic conditions than for the subsonic ones. Additionally, a shift in the moment is appreciated at 30^{o} for subsonic conditions, probably caused by the detachment of the boundary layer. This effect was not observed for the supersonic case, but only because it was not possible to reach angles of attack greater than 28^{o} and attaining convergence.

It should also be noted that, even though the observed values for the pitch moment are positive, the used sign criteria takes it as positive by the right hand rule applied on a Y-axis which coincides with the left wing. This is notoriously opposite to the conventional sign criteria used in (for example) Flight Mechanics and indicates that, the greater the angle of attack, the greater the moment exherted by the wing to return to the 0^{o} position, thus making it stable in this regard.

6.b Validation of Results

For the validation of the obtained results by means of the performed CFD simulations, a number of different sources were consulted. Thus, the values presented in Table 7 were found in the consulted bibliography for the Concorde's performance. It should be noted that, regarding the "Hold" conditions, nothing is stated in the consulted source, so they are taken as the values for a holding pattern with no deflection from any control surface or flaps, while keeping in mind that this might not necessarily be the case.

Flight Regime	C_L [29]	AE [29]	AE [30]
Supersonic Cruise	0.125	7.14	7.5
Hold at 250 kts and 10'000 ft	0.28	9.27	-

Table 7: Table with values found in the bibliography for the Concorde for different flight regimes and sources.

Should we compare the data presented in Table 7 to the one shown in Figures 10 and 19, it is then possible to see the following:

- The lift coefficient and aerodynamic efficiency in supersonic conditions take the value presented in the table for angles of attack of around 10^{o} and 5^{o}, respectively. Even though the consulted sources do not state under which circumstances the reference values are attained, it would seem strange that they are given for two completely different angles of attack. It should also be pointed out that, when computing the aerodynamic efficiency, the drag referred to the fuselage and stabiliser were not computed (since the used 3D model is of only the wing), so it is probable that the actual computed aerodynamic efficiency is lower in reality.

- The lift coefficient and aerodynamic efficiency in subsonic conditions (which roughly equate in terms of velocity, but not altitude, to the ones used in the simulations) take values close to the ones of the table at angles of attack of around 15^{o} and 6^{o}. Once again, it seems strange that the incidences at which this is achieved do not coincide, and the computed aerodynamic efficiency should be smaller due to the already explained reasons.

Additionally, the maximum aerodynamic efficiency in supersonic conditions can be calculated by means of the following formula, such that, for the considered flight conditions, it has a value of [31]:

$$AE_{C,max} = \frac{L}{D} = \frac{C_L}{C_D} = \frac{4 \cdot (M_C + 3)}{M_C} = 9.901; \tag{3}$$

The evaluation of Figure 19 allows to conclude that this maximum value is not achieved at all, specially if we take into account that the fuselage was not considered.

The study of the available bibliography also lead to the following polar curve (lift versus drag coefficients) being obtained for the wing of the Concorde in supesonic conditions, which can be compared to a similar curve that was obtained for the calculated results:

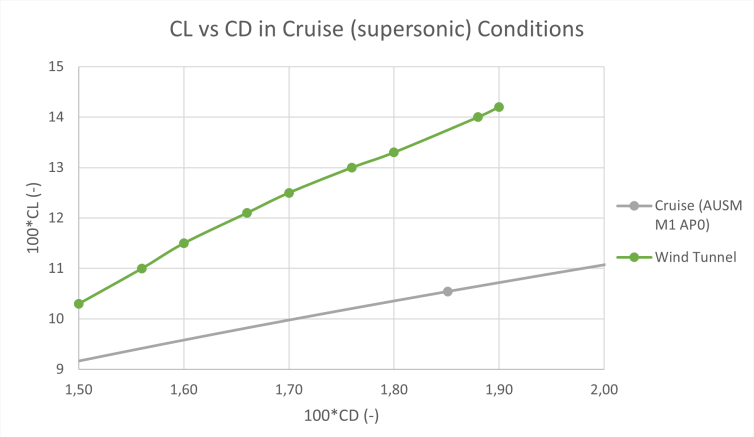

Figure 21: Graph representing the values of the lift coefficient against those of the drag coefficient for supersonic flight conditions for the obtained results, and for the Concorde's production models in wind tunnel testing.[32].

Comparing them allows to see that the theoretical tendency is not followed by the results provided by the CFD study. Nonetheless, it should be pointed out that, for the range of values in question, only a single data point can be studied after zooming in on the polar curve (which can be observed in a more general shape in Figure 22a).

Another source was consulted and the general polar curve for supersonic conditions obtained, being presented together with the polar curve for the results of the simulations below:

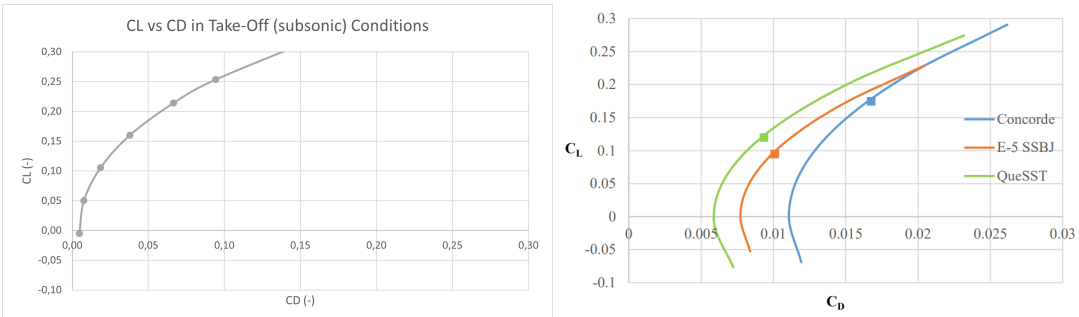

(a) 20a (b) 20b

Figure 22: (from left to right) Graphs representing the values of the lift coefficient against those of the drag coefficient for supersonic flight conditions for the obtained results, and for a study of the aerodynamics of the Concorde, E-5 SSBJ and QueSST supersonic aircraft.[33]

Once again, the comparison of these two graphs leads to a similar conclusion as before:t the obtained results do not match those found in the bibliography that should allow to validate them.

Nonetheless, it should be pointed out that, should one contrast Figure 21 and the region corresponding to this case at 22b, it is then clear to see that none of them present values that are close to each other, which puts into question the validity of any of these sources. Given that the former is a graph obtained from wind tunnel testing of a Concorde model done by BAC and Aéroespatiale, while the latter comes from a CFD study of the aerodynamic performance of various supersonic aircraft, the first of the two should be taken as the most reliable of the two sources. In any case, except for the overall shape of the curve, the behaviour of the obtained results is quite far from the ones to be expected.

Overall, it is clear to see that the performed CFD study does not provide results that completely match the data obtained by the bibliographical review. This can be attributed to a number of reasons, other than the fact that the obtained results are inaccurate due to the coarseness of the mesh, among which we can cite:

- The fact that the fuselage and stabilizer are not being considered at all. This would obviously affect the aircraft's performance, specially with regards to the drag coefficient, but also with respect to the lift and pitch moment coefficients, since the fuselage, by virtue of being a slender body, would generate some lifting force and pitch moment due to cross-flow (3D effects) and also due to the vortices generated by the flow. [34] This effect should be negligible when compared to that of the wings (since this phenomena is mainly present in missiles and other slender bodies), but it might be one of the causes for the disparity between the data. Additionally, the absence of the fuselage in the supersonic simulations might be affecting considerably the obtained results, since the nose of the aircraft would be the first point in the geometry where a shock-wave would form, thus affecting the flow that is downstream from it, which could have an effect on the overall wing aerodynamic behaviour.

- For some of the same reasons, the fact that the engine nacelles were done away with when curating the 3D model to reduce the computational power needed to solve the flow around the wing, may have resulted in the behaviour of the flow around the wing not being properly modelled. This is specially true because of the shape of the nacelles, which should slow down considerably the flow around them, as we have already seen in Section 6.a.

- Nothing is noted in none of the consulted sources regarding how the different coefficients were computed with respect to the measured forces. This is specially important, since the use of a reference surface other than the wing surface (used along this study) might lead to results differing noticeably. Nonetheless, this should not affect at all the aerodynamic efficiency, and it would then lead to results that are noticeably different, and not close to the ones obtained.

In any case, the fact that the used mesh is too coarse and not very good and the fact that some imperfections that were not perceived might have been left in the used 3D CAD after curating it, may also be a very important cause why the evaluation of any of the data related to the drag coefficient (C_L vs C_D curves and the aerodynamic efficiency) does not coincide with the results that we should be theoretically obtaining.

Additionally, the lack of data in any of the consulted sources regarding the pitch moment coefficient made it impossible to validate the results regarding this variable. In any case, since the results for the other coefficients seemed to be quite far from what was to be expected, it is then safe to assume that the results for it would not be reflecting the real aerodynamic behaviour of the Concorde's wing.

7 Conclusion

In conclusion, throughout this document, the overall process followed for the evaluation in CFD of the aerodynamic properties of the wing of the Aéroespatiale-BAC Concorde is presented. Said process consisted in the acquisition and curation of a simplified 3D model, which was then used as a base to design the domain to be used for the calculations, followed by the design of an initial mesh that was employed as a base to evaluate convergence and mesh independence. Said mesh, due to computing power, time and knowledge constraints, had to be used to obtain the results that were later evaluated and compared to real-life and theoretical data regarding the Concorde's aerodynamic performance, showing that the overall CFD analysis did not provide very accurate results, together with the reasons why this could be happening.

All in all, even if the main conclusions that could be extracted from this Thesis are that the overall CFD study should be repeated with a better and smoother 3D model which has a mesh presenting a Prism Layer Mesher from the very beginning and with more computing power available, the lessons regarding how to work with CFD tools, specially with Star-CCM+, that the student obtained throughout the realisation of this study should not be understated.

References

[1] Britannica, *Concorde*, https://www.britannica.com/technology/Concorde.

[2] Airlines Inform, *Concorde*, https://www.airlines-inform.com/commercial-aircraft/concorde.html.

[3] Orlebar, Christopher, *The Concorde Story*.

[4] British Airways, *Celebrating Concorde*, https://www.britishairways.com/es-es/information/about-ba/history-and-heritage/celebrating-concorde.

[5] Digital Dutch, *1976 Standard Atmospheric Calculator*, https://www.digitaldutch.com/atmoscalc/.

[6] Aisak, *Proyect Concorde (Unfinished) - GrabCad.com*, https://grabcad.com/library/proyect-concorde-unfinished-1.

[7] Jain, Rohit; Jain, Sandeep; Bajpai, Lokesh; *Aerodynamics of Winglet: A Computational Fluid Dynamics Study Using Fluent*.

[8] Recalenda, Edoardo; *Analysis of three different Winglet models with comparison between CFD simulation and wind tunnel testing*.

[9] Ferrero Micó, Javier; *CFD study and manufacturing of a wing with winglets*.

[10] Cakir, Mustafa; *CFD study on aerodynamic effects of a rear wing/spoiler on a passenger vehicle*

[11] Gómez-Aldaraví, Pedro Martí; Navarro García, Roberto; *Unit 10 - Introduction to Turbulence*; Computational Fluid Mechanics Extension; Aerospace Engineering Degree - Universidad Politécnica de Valencia.

[12] P. Panagiotou, P. Kaparos, K. Yakinthos; *Winglet design and optimization for a MALE UAV using CFD*.

[13] Madhanraj, V.; Ganesh Chandra, Kaka; Swprazeeth, Desineni; Dhanush Gopal, Battina; *Design and Computational Analysis of Winglets*.

[14] Segui, Marine; Abel, Federico R.; Botez 1, Ruxandra M.; Ceruti, Alessandro; *New aerodynamic studies of an adaptive winglet application*.

[15] Abid Mahmood, Chowdhury; Kumar Das, Ratan; *Performance comparison of different winglets by CFD*.

[16] Guerrero, J.E.; Sanguineti, M.; Wittkowski, K.; *Variable cant angle winglets for improvement of aircraft flight performance*.

[17] Abdellatif, Osama; Khalil, E. E.; Said, Eslam; *Winglet Cant and Sweep Angles Effect on Aircraft Wing Performance*.

[18] Ueyama, Atsushi; Hexagon; *Basic Course of Thermo-Fluid Analysis 06: Chapter 3 Basics of Flow - 3.2.1 Compressible/incompressible fluids*; https://www.cradle-cfd.com/media/column/a70#:~:text=For%20fluid%20velocities%20less%20than,during%20volume%20expansion%20or%20compression.

[19] Engineering.com, *3 Criteria for Assessing CFD Convergence*, https://www.engineering.com/story/3-criteria-for-assessing-cfd-convergence

[20] ResearchGate, *How to Set Angle of Attack for Airfoil Simulation?*, https://www.researchgate.net/post/How-to-Set-Angle-of-Attack-for-Airfoil-Simulation.

[21] CFD Online, *Changing the Angle of Attack in Star-ccm+*, https://www.cfd-online.com/Forums/star-ccm/150626-changing-angle-attack-star-ccm.html#:~:text=If%20you%20must%20rotate%20the,part%20and%20select%20transform%20%3E%20rotate.

[22] Rom, Josef; *High Angle of Attack Aerodynamics : Subsonic, Transonic, and Supersonic Flows*.

[23] CFD Online, *Sutherland's Law*, https://www.cfd-online.com/Wiki/Sutherland%27s_law.

[24] Auxiliary Star-CCM+ Documentation, *Evaluation of Inviscid Fluxes*.

[25] Gómez-Aldaraví, Pedro Martí; Navarro García, Roberto; *Unit 9 - CFD post-processing*; Computational Fluid Mechanics Extension; Aerospace Engineering Degree - Universidad Politécnica de Valencia.

[26] LEAP Australia; *TIPS & TRICKS: CONVERGENCE AND MESH INDEPENDENCE STUDY*; https://www.computationalfluiddynamics.com.au/convergence-and-mesh-independent-study/.

[27] Aerospaceweb, *Applying the Lift Equation*, https://aerospaceweb.org/question/aerodynamics/q0252.shtml.

[28] Bashiera Hamizi, Ilya; Afghan Khan, Sher; *CFD Letters Aerodynamics Investigation of Delta Wing at Low Reynold's Number*.

[29] Concorde Celebrating an Aviation Icon, *Concorde Technical Specs*, https://www.concordesst.com/concordeb.html.

[30] Candiel, Sébastien; *Concorde and the Future of Supersonic Transport*.

[31] fx Solver, *Supersonic/Hypersonic Lift-to-Drag Ratio*, https://www.fxsolver.com/browse/formulas/Supersonic%5CHypersonic+Lift-to-Drag+Ratio.

[32] Leyman, C. S; Rech, J.; Aerospatiale; British Aerospace; *A case study by Aerospatiale and British Aerospace on the Concorde*.

[33] Sun, Yicheng; Smith, Howard; *Sonic Boom and Drag Evaluation of Supersonic Jet Concepts*.

[34] Nielsen, Jack N.; *Missile Aerodynamics*.

[35] Autodesk; *Fusion 360 plans and pricing*, https://www.autodesk.com/campaigns/fusion-360/pricing?term=1-MONTH&tab=subscription.

[36] United Nations - Department of Economic and Social Affairs; *THE 17 GOALS*, https://sdgs.un.org/goals#.

A Articles and Conditions

The main purpose of this Appendix is to discuss all the laws and regulations applied and contemplated throughout the development of this project, which are given by the different Royal Decrees (*Reales Decretos* in Spanish) and Directives related to working conditions. All of the presented dispositions and rules were followed when performing this Thesis.

A.a Royal Decree 486/1997 (Real Decreto 486/1997)

This document is basically a transposition to Spanish law of the contents of Directive 86/654/EEC of November 30th of the European Union. The main points contemplated in it that relate to this project are hereby discussed.

A.a.1 Structural Security

In this matter, the following issues are contemplated:

- Workplace dimensions should allow for the correct development of the task at hand without risks for health and security, and in acceptable ergonomic conditions. Its minimum dimensions are to be: 2.5 m in height from the floor to the ceiling, 2 m^2 of free surface and 10 m^3 of space per worker.
- Separation between material elements present in the workplace must be enough so that the workers might be able to execute their labour in a safe, healthy and correct manner.
- Workers should be able of safely open, close, adjust or fixate windows, illumination vanes and ventilation devices.
- Staircases should have a minimum width of 1 m, being the steps of the same dimensions, and handrails be present at the open sides if the height is greater than 60 cm.
- All evacuation exits must remain clear and lead as directly as possible to a safe zone, and in case of danger workers must be able to evacuate the workplace fast and safely.

A.a.2 Order, Cleanliness and Maintenance

Being the main disposition that the workplaces should be periodically cleaned and whenever necessary to maintain at all times adequate hygiene conditions.

A.a.3 Workplace Environmental Conditions

The exposition to the environmental conditions of the workplace should not constitute a hazard to the safety and health of the workers, nor should it be a source of discomfort or inconvenience. To this effect, extreme temperatures and humidities, sudden changes in temperature, annoying air currents, unpleasant smells and excessive irradiation ought to be avoided.

A.a.4 Workplace Lighting

In this regard, the main dispositions are:

- Workplace lighting should conform to the characteristics of the task to be performed.
- Whenever possible, workplaces will have natural lighting which will be compensated with artificial lighting whenever the former is not enough.

A.b Royal Decree 488/1997 (Real Decreto 486/1997)

This document consists on the transposition to Spanish law of the contents of Directive 90/270/EEC of May 29th of the European Union. The main points contemplated in it that relate to this project are hereby discussed.

A.b.1 Equipment

With regards to the equipment to be used, the following is of interest:

- Screen: must be orientable or easily tilted, and the lighting and contrast between the characters and the backgroung of the screen must be easily adjusted to adapt to the user's needs.
- Keyboard: must have enough space in front of it so that the user can rest their arms and hands, and the symbols and keys must be readable from a regular working position.
- Desk or work surface: must have enough space to allow the worker a comfortable position, as well as a flexible disposition of the different work elements.
- Work seat: must have adjustable height and its backrest should be tiltable and of adjustable height.

A.b.2 Surroundings

Last, but not least, when referring to the surroundings, the main points to keep in mind are the following:

- Space: the workplace must have enough dimensions and be conditioned in such a way that there is enough space to allow for changes in posture and work movements.
- Lighting: there must be lighting levels and adequate luminance relations between the screen and the surroundings.
- Reflections and Glares: workplaces must be installed in such a way that light sources do not cause direct glare nor reflections. Furthermore, windows must be equipped with an adjustable covering device to attenuate the daylight lighting the workplace.

B Budget

Throughout this appendix, all the costs related to the development of this project are explained in order to be able to estimate how much would it cost for an aeronautics related firm or laboratory to replicate this Thesis. To do this, we will first discuss the individual costs of all of the different assets and, then, add them all up to obtain the total cost of the project.

In this project, like for any other, we can distinguish between two main types of assets, which are:

- Human assets: as their name indicates, this is referred to all of the individuals that contributed some of their time to perform this project. Among these, we highlight:
  - The author of this Thesis (an Aerospace Engineering Degree student).
  - The tutor of this Thesis (Xandra Marcelle Margot).
- Material assets: this category is formed by any other used asset that does fall into the first one. We will mainly be speaking of:
  - Software licenses. Throughout this project, the main softwares used were Fusion360 and Star-CCM+. The former was used for the adaptation of the 3D model, while the latter was used for the CFD simulations.
  - Hardware (the computer used to perform all simulations and any other operation).
  - Electrical power used during this project, since any piece of electronic hardware requires electricity to run.

Having discussed all of the different assets that were needed to perform this project, it is then possible to start discussing the overall time that was invested for the different aspects of the project and the costs related to each of them.

When it comes to discussing the hourly cost of each of the man-hours put by the author into this project, this was calculated by taking the average salary that a junior engineer would have when recently contracted in an engineering firm or research facility. Said salary was indicated by the tutor to be of around 33€ per hour. Therefore, all costs related to his work are presented as follows:

Item	Measurement (h)	Unitary Cost (€/h)	Total Cost (€)
Author - Research	50	33	1'650
Author - 3D Model Curating	25	33	825
Author - CFD Work	125	33	4'125
Author - Writing and Correction	100	33	3'300
Author - Total	300	33	9'900

Table 8: Table with the estimated costs related to all the work performed by the author of this Thesis.

It should be noted that the last row on Table 8 refers to the total monetary cost of the author's work. Moving on then, the other costs could be discussed in a similar way.

Item	Measurement (h)	Unitary Cost (€/h)	Total Cost (€)
Tutor - Tutorials	14	50	600
Tutor - Review	16	50	800
Tutor - Total	30	50	1'500

Table 9: Table with the estimated costs related to all the work performed by the tutor of this Thesis.

Following a similar process, the partial costs related to the used software are presented in Table 10. It should however be noted that, in this case, the cost of the use of Star-CCM+ is measured in hours (taking

into account that a license costs around 180 k€ per year and that a year has 365 days and 6 hours, as indicated by the tutor), while the use of Fusion360 is measured in months, since this is the smallest overall payment plan that Autodesk allows for. Nonetheless, it should be pointed that Fusion360 was used because the student had free access to it thanks to a university-provided license.

Item	Measurement	Unitary Cost	Total Cost (€)
Software - Star-CCM+	506 h	20.53 €/h	10'390
Software - Fusion360	1 Unit (month)	65 €/month [35]	65
Software - Total	-	-	10'455

Table 10: Table with the estimated costs related to all the time invested using all of the different softwares employed in this Thesis.

After this, only the cost of the hardware and consumed power remained, which are presented in much of a similar manner in Table 11. It should be noted that the overall laptop cost was taken as the price paid when it was bought, since it was not acquired specifically to perform this project. On the other hand, to calculate the overall power cost, the average power consumption in the student's household for 2023 from January to May was taken as reference.

Item	Measurement	Unitary Cost	Total Cost (€)
Hardware - Laptop	1 Unit	1'100 €/Unit	1'100 €
Hardware - Power	806 h	0.08 €/h	62.59
Hardware - Total	-	-	1'163

Table 11: Table with the estimated costs related to the laptop used and power consumed while doing this Thesis.

Therefore, the total costs of the project can be summarised in the following table:

Item	Total Cost (€)
Author - Total	9'900
Tutor - Total	1'500
Software - Total	10'455
Hardware - Total	1'163
Total Cost	23'018

Table 12: Table with the estimated total costs recquired for developing this Thesis.

C Relation to the 2030 Sustainable Development Goals

In this last appendix, the relation of the developed project to the 2030 Sustainable Development Goals (SDGs) is made. Due to it being of mainly academic nature and based around using a CFD software to evaluate the aerodynamics of the wing of a supersonic aircraft that is no longer in use to increase the author's knowledge in the use of this tool, none of the SDGs apply to it, as it is reflected in Table 13.

We could further indicate that the majority of the Goals (1 through 6, as well as 8, 10, 11 and 14 through 17) do not really apply to the main fields of study and/or work of the Aerospace Engineering degree, except number 16, which would be affected by its defense and military applications. Of the ones left:

- SDG 7 would only apply if the subject of this project was the use or implementation of some kind of new propulsion system that was more environmentally-friendly than the widely-used oil derived fuels, like hydrogen, bio-fuels or electric propulsion, amongst others. Since this is not the case, the relation of this project to this goal does not really apply.
- SDG 9 is mainly related to industrialisation and infrastructure. Since in this project neither a real attempt is being made at discussing the manufacture of an aicraft using the obtained data, advocating for its reintroduction, nor trying to design airports and similar infrastructure around it, we can also see that it does not apply.
- SDG 12 revolves around production techniques and, for similar reasons as the ones explained for SDG 9, it does not apply to this project.
- SDG 13 focuses on climate action and combating climate change. Due to the issues described for SDG 7 and 9, it is also clear to see that it is not related at all to this project.

It should, however, be noted that, if a more in depth study was to be performed using more powerful computers that allowed for finer meshing and better convergence of all the simulations, a case could be made regarding production and climate action (SDGs 12 and 13, respectively).

The main reason for this would be the fact that, said computers would have to be produced and bought (unless they were already owned by the institution that was going to perform the study) and supplied with constant power for long periods of time while they calculate.

As such, an argument could be made about the need to find clean and affordable energy sources and maybe recycling computer components or materials to make sure that this hypothetical study is performed in the most environmentally-friendly way and consuming as little resources as possible.

Nonetheless, since this is all hypothetical, these goals do not strictly apply to the project that has been developed and presented along this document. Henceforth, in the following table a short summary of how all the SDGs relate to it are presented, with the corresponding field being marked with an "X":

Sustainable Development Goals (SDGs)	High	Medium	Low	Does Not Apply
SDG 1. **No Poverty**	-	-	-	X
SDG 2. **Zero Hunger**	-	-	-	X
SDG 3. **Good Health and Well-Being**	-	-	-	X
SDG 4. **Quality Education**	-	-	-	X
SDG 5. **Gender Equality**	-	-	-	X
SDG 6. **Clean Water and Sanitation**	-	-	-	X
SDG 7. **Affordable and Clean Energy**	-	-	-	X
SDG 8. **Decent Work and Economic Growth**	-	-	-	X
SDG 9. **Industry, Innovation and Infrastructure**	-	-	-	X
SDG 10. **Reduced Inequalities**	-	-	-	X
SDG 11. **Sustainable Cities and Communities**	-	-	-	X
SDG 12. **Responsible Consumption and Production**	-	-	-	X
SDG 13. **Climate Action**	-	-	-	X
SDG 14. **Life Below Water**	-	-	-	X
SDG 15. **Life on Land**	-	-	-	X
SDG 16. **Peace, Justice and Strong Institutions**	-	-	-	X
SDG 17. **Partnerships for the Goals**	-	-	-	X

Table 13: Table with the estimation of how the performed project is related to each of the 2030 SDGs.[36]